Bayesian Asteroseismology of 23 Solar-Like Kepler Targets

M. Gruberbauer[1]⋆, D.B. Guenther[1]†, K. MacLeod[1]‡ T. Kallinger[2]§

[1]*Institute for Computational Astrophysics, Department of Astronomy and Physics, Saint Mary's University, Halifax, NS B3H 3C3, Canada*
[2]*Institute for Astrophysics, University of Vienna, Türkenschanzstrasse 17, A-1180 Vienna, Austria*

ABSTRACT

We study 23 previously published Kepler targets to perform a consistent grid-based Bayesian asteroseismic analysis and compare our results to those obtained via the Asteroseismic Modelling Portal (AMP). We find differences in the derived stellar parameters of many targets and their uncertainties. While some of these differences can be attributed to systematic effects between stellar evolutionary models, we show that the different methodologies deliver incompatible uncertainties for some parameters. Using non-adiabatic models and our capability to measure surface effects, we also investigate the dependency of these surface effects on the stellar parameters. Our results suggest a dependence of the magnitude of the surface effect on the mixing length parameter which also, but only minimally, affects the determination of stellar parameters. While some stars in our sample show no surface effect at all, the most significant surface effects are found for stars that are close to the Sun's position in the HR diagram.

Key words: stars:oscillations – methods:statistical

1 INTRODUCTION

Ultra-precise long-term photometric time series from space have revolutionized the study of stellar variability in recent years. The CoRoT (Michel et al. 2008) and the *Kepler* (Borucki et al. 2010) space telescopes in particular have produced high-quality data sets for thousands of stars in order to detect planets down to Earth size and below. Particularly interesting for the study of stellar interiors and stellar evolution is their ability to detect solar-type oscillations from giants to subdwarfs. The pulsational characteristics of these stars adhere, at least to a very good first approximation, to scaling relations (e.g., Huber et al. 2011) permitting the study of large populations of stars with "ensemble asteroseismology" (Chaplin et al. 2011) and even Galactic archeology (Miglio et al. 2013).

The same information can also be exploited to infer the parameters of individual stars, e.g., to better constrain their planets' properties. For stellar astrophysics, however, the ultimate goal is to use asteroseismology to study stellar interiors. Instead of direct inversion of the pulsation information, asteroseismology usually employs a comparison between observed and modelled pulsation frequencies (e.g., Guenther & Brown 2004). Various new tools have been

developed to facilitate a state-of-the-art version of such a comparison using different approaches, such as the Asteroseismic Modelling Portal (AMP) (Metcalfe et al. 2009) and Bayesian grid-based analysis (Gruberbauer et al. 2012, hereafter Paper I). The major differences between these methods lie in their different statistical basis and their different applications of what is known as the surface effect correction (see Paper I for an in-depth discussion). Already, the AMP has been used to analyse some Kepler targets in detail and to compare the results with those from other modellers (Metcalfe et al. 2010, 2012). Such a comparison is advantageous, because asteroseismic modelling often relies on a specific set of stellar models with a specific set of input physics. Slight systematic differences among these models are therefore not only plausible but unavoidable, resulting in underestimated uncertainties. A different approach is to study a larger sample of stars self-consistently with one particular method and model base to facilitate a pool of results to be compared with other researcher's results (Mathur et al. 2012).

In this paper we reexamine some of the previously published studies based on Kepler data with a strong emphasis on AMP results, employing our own set of models and our Bayesian method described in Paper I. We will discuss how the results differ and whether the methodologies themselves introduce systematic deviations. We will also perform the first detailed study on surface effects for a sample of stars with our flexible method.

⋆ E-mail: mgruberbauer@ap.smu.ca
† E-mail: guenther@ap.smu.ca
‡ E-mail: kmacleod@mars.smu.ca
§ E-mail: thomas.kallinger@univie.ac.at

2   METHODS, MODELS AND OBSERVATIONS

2.1   Target selection and observations

In order to investigate the impact of the stellar models and methodologies in the most general sense, we analyse stars for which the p-mode frequency sets and detailed prior information used in previous asteroseismic fitting procedures are available in the literature. We furthermore constrain ourselves to stars that do not show strong signatures of deviations from the asymptotic relation, i.e., avoided crossings such as in KIC 11026764 (Metcalfe et al. 2010). While those signatures are very valuable for asteroseismic inferences and can be easily taken into account with our method as mentioned in Paper I, they would constitute special cases in the comparison between methods. We therefore postpone such an analysis to a future paper and restricted ourselves to 20 of the 22 stars analysed by Mathur et al. (2012) (hereafter Mathur20), the solar analogues 16 Cyg A & B (Metcalfe et al. 2012), and the planet-host Kepler-36 (Carter et al. 2012). Where available in the previously cited papers, we use prior constraints on $\log T_{\rm eff}$, $\log L/L_\odot$, Z/X (adopting $[{\rm Fe/H}]_\odot = 0.0245$) and $\log g$. Following our description in Paper I, these prior constraints are modelled as separate Gaussian probability distributions.

As is common in recent asteroseismic analyses, we treat the frequency of maximum power $\nu_{\rm max}$ as an additional and independent observable by using the scaling relation

$$\nu_{\rm max,mod} \approx \frac{M/M_\odot \, (T_{\rm eff}/T_{\rm eff,\odot})^{3.5}}{L/L_\odot} \nu_{\rm max,\odot}. \qquad (1)$$

where we employ the solar value $\nu_{\rm max,\odot} = 3120.0 \pm 5\,\mu{\rm Hz}$ given by Kallinger et al. (2010) based on VIRGO data. For Mathur20, the observed values and uncertainties of $\nu_{\rm max}$ have been taken from Mathur et al. (2012), and for Kepler-36 we have used the value published in Carter et al. (2012). For 16 Cyg A & B, we have determined the values ourselves by performing a Bayesian multi-component model fit, consisting of a flat background, three super-Lorentzian profiles and a Gaussian power hump, to the power density spectra of both data sets[1]. In this case, the central frequency of the Gaussian power hump and the corresponding uncertainties are interpreted as a good proxy for $\nu_{\rm max}$. The method employs the nested sampling algorithm MultiNest (Feroz et al. 2009) and is described in more detail in Kallinger et al. (2010). We find $\nu_{\rm max} = 2215.6 \pm 6.5\,\mu{\rm Hz}$ for 16 Cyg A, and $\nu_{\rm max} = 2571.9 \pm 12.6\,\mu{\rm Hz}$ for 16 Cyg B.

2.2   Models

A wide parameter range has to be spanned in order to perform a meaningful grid-based analysis. We therefore employed YREC (Demarque et al. 2008) to produce a set of dense grids covering a wide range in initial masses, and several values for the initial helium mass fraction Y_0, initial metal mass fraction Z_0, and mixing length parameter $\alpha_{\rm ml}$.

---

[1] Note that only Q7 data obtained between September 2010 to December 2010 have been used in Metcalfe et al. (2012). We therefore restrict ourselves to this data set as well.

Our model tracks begin as completely convective Lane-Emden spheres (Lane 1869; Chandrasekhar 1957) with the stellar age reset to zero when the star crosses the birthline ($10^{-5}\,{\rm M}_\odot/{\rm yr}$, Palla & Stahler 1999). They are evolved from the Hayashi track (Hayashi 1961) through the zero-age-main-sequence (ZAMS) to the base of the red giant branch. Constitutive physics include the OPAL98 (Iglesias & Rogers 1996) and Alexander & Ferguson (1994) opacity tables, as well as the Lawrence Livermore 2005 equation of state tables (Rogers 1986; Rogers et al. 1996). Convective energy transport was modelled using the Böhm-Vitense mixing-length theory (Böhm-Vitense 1958, MLT,). The atmosphere is implemented using Eddington gray atmosphere. Nuclear reaction cross-sections were taken from Bahcall et al. (2001) and the nuclear reaction rates from Table 21 in Bahcall & Ulrich (1988). The effects of helium and heavy element diffusion (Bahcall et al. 1995) were included. The model grid contains models with $M/M_\odot$ from 0.8 to 1.3 in steps of 0.01 and Y_0 from 0.210 to 0.315 in steps of 0.005. Furthermore, Z_0 is varied from 0.005 to 0.04 in steps of 0.005, but with the overall constraint that $X_0 \geqslant 0.68$. Lastly, we also vary $\alpha_{\rm ml}$ from 1.8 to 2.4 in steps of 0.1.

The pulsation spectra were computed using the stellar pulsation code of Guenther (1994), which solves the linearized, non-radial, non-adiabatic pulsation equations using the Henyey relaxation method. The non-adiabatic solutions include radiative energy gains and losses but do not include the effects of convection. We estimate the random 1σ uncertainties of our model frequencies to be of the order of $0.1\,\mu{\rm Hz}$. These uncertainties are properly propagated into all further calculations.

2.3   Bayesian asteroseismic grid fitting

Our Bayesian fitting method is explained in detail in Paper I, and it has been previously applied to analyse the Sun (Gruberbauer & Guenther 2013). We compare theoretical ($f_{\rm m}$) and observed ($f_{\rm o}$) frequencies by calculating the likelihood that the two values agree were it not for the presence of random and systematic errors, i.e.,

$$f_{\rm o} - f_{\rm m} = \gamma\Delta + e. \qquad (2)$$

Here, the random errors e are assumed to be independent and Gaussian. The systematic errors $\gamma\Delta$ in the case of solar-like stars are assumed to be similar to "surface effects". At higher orders, observed frequencies are systematically lower than model frequencies, and the absolute frequency differences increase with frequency. This is modelled by introducing Δ as free parameters for each observed mode and by setting $\gamma = -1$.

These Δ terms are then allowed to become larger at higher radial orders. The upper limit $\Delta_{\rm max}$ for each model frequency $f_{\rm m}$ is determined by the large frequency separation and a power law similar to the standard correction introduced by Kjeldsen et al. (2008) so that

$$\Delta_{\rm max} = \Delta\nu \left(\frac{f_{\rm m}}{f_{\rm max,m}} \right)^b, \qquad (3)$$

where $b = 4.9$, $\Delta\nu$ is the large frequency separation of the

corresponding model, and $f_{\mathrm{max,m}}$ is the frequency of the highest order in the model[2].

The Δ parameter is incorporated in a completely Bayesian fashion, using a β prior to prefer smaller values over larger ones (see Paper I for more details). In addition, we always allow for the possibility that a mode is not significantly affected by any kind of systematic error by explicitly including the null hypothesis, that is by combining the probabilities of two hypotheses: one with and one without the Δ parameter. Altogether, this allows us to fully propagate uncertainties originating from the surface effects, or other potential systematic differences, into all our results. At the same time it gives us more flexibility than the standard surface-effect correction. Whereas the latter prescribes a fixed power-law behaviour for the actual surface effects, our method only prescribes such a behaviour for the *upper limits* of the surface effects for the individual radial model frequencies.

For each model in our grid, all the likelihood terms from the different frequencies are combined to yield an overall weighted likelihood for the model, where the weights are provided either via prior information or using ignorance priors (i.e., information that simply encodes the dimension of the grid). These weights provide correctly normalized probabilities that allow us to derive distributions for all model properties (e.g., mass, age, fractional radius of the base of the convection zone R_{BCZ}, mixing-length parameter α_{ML}, and so on).

In summary, we obtain probabilities for every evolutionary track in our grid, and within the tracks also for every model. We also obtain the correctly propagated distributions for systematic errors so that the model-dependent surface effect can be measured. In order to fully resolve the changes in stellar parameters and details in the stellar-model mode spectra, we oversample the evolutionary tracks via linear interpolation until the (normalised) probabilities no longer change significantly. Eventually, we obtain so-called evidence values, equivalent to the prior-weighted average likelihood, for the grid as a whole. These could, in principle, be used to perform a quantitative evaluation of different input physics (see Gruberbauer & Guenther 2013) or even different stellar evolution and pulsation codes. We will use them in this study to analyse the significance of the measured surface effects.

In order to facilitate this, we propose two alternative systematic error models in addition to the standard surface effect (SSE) model described above. First, we employ a less restrictive systematic error model where

$$\Delta_{\mathrm{max}} = \Delta\nu/2 \qquad (4)$$

for every frequency of each particular model. Furthermore, the observed frequencies are allowed to deviate in either direction (first $\gamma = 1$ is evaluated, then $\gamma = -1$ follows, and then both results are combined using the sum rule). We call this model the "arbitrary systematic error" (ASE) model since it allows, in principle, very large differences between observed and calculated frequencies without prescribing any

systematic behaviour or preferred sign. Note that this is not equivalent to simply increasing the Gaussian uncertainties of the observed frequencies to $\Delta\nu/2$.

Finally, we will also employ a third error model which only consists of the probabilities obtained without any Δ parameters. This model therefore assumes that no systematic errors are present so that $f_{\mathrm{o}} - f_{\mathrm{m}} = e$. We will call this the "no systematic error" (NSE) model. Together, the three systematic error models will allow us to estimate the significance of surface effects or other systematic differences between observed and calculated frequencies.

## 3 DEPENDENCE OF SURFACE EFFECTS ON NON-ADIABATICITY AND MIXING LENGTH

The advantage of our method to include systematic frequency errors over the standard surface correction is its universality. The standard surface effect exponent of $b = 4.9$ as obtained by Kjeldsen et al. (2008) has been derived for adiabatic pulsation frequencies and for a solar-calibrated model with a calibrated parametrization of the mixing length[3]. More advanced pulsation models and different stellar models (see, e.g., Grigahcène et al. 2012) are not necessarily consistent with such a relation. This is also the case for our non-adiabatic pulsation frequencies. Since the only way to improve our modelling of outer layers is to compare more advanced models to observations, it is necessary to relax the constraint of a definite empirical surface correction relation dependent on adiabatic pulsation codes. Aside from the surface effect, our method also allows various other kind of parameterisation for systematic errors, such as our ASE model.

The drawback of our method, as discussed in Paper I, is that in the absence of strong prior information about the stellar parameters, a lack of lower-order modes will potentially result in an underestimated magnitude of the surface effects. This follows from the fact that we always obtain the most probable result given our state of information including the new data set; if we cannot constrain the stellar model parameters using our prior knowledge, the pulsation frequencies are our only reference. When conditions are encountered under which the empirical correction law of Kjeldsen et al. (2008) does not apply, or if one rejects such a correction on other grounds, we have to evaluate the models acknowledging the presence of less well-specified systematic errors.

As described in Paper I, neglecting lower order modes leads to overestimated α_{ml}, mass, and metallicity for the Sun, simply because such models can fit the higher order modes better. The same models cannot fit the lower order modes as well, but when they are not included in the list of fitted modes no penalty ensues. For stars other than the Sun, we usually do not have a complete list of lower-order modes, nor do we have as accurate non-seismic constraints (e.g., mass, luminosity, age). Even in such cases, however, stellar

---

[2] This means that for the highest order in the model $\Delta_{\mathrm{max}} = \Delta\nu$ and guarantees that we do not introduce ambiguities in the radial orders by implementing the Δ terms.

[3] As explained in the previous section, technically we also use $b = 4.9$ for our surface effect modelling, but the exponent is only employed to derive an upper limit for the surface effect for each mode. This does not enforce the usual power-law like behaviour of the surface effect.
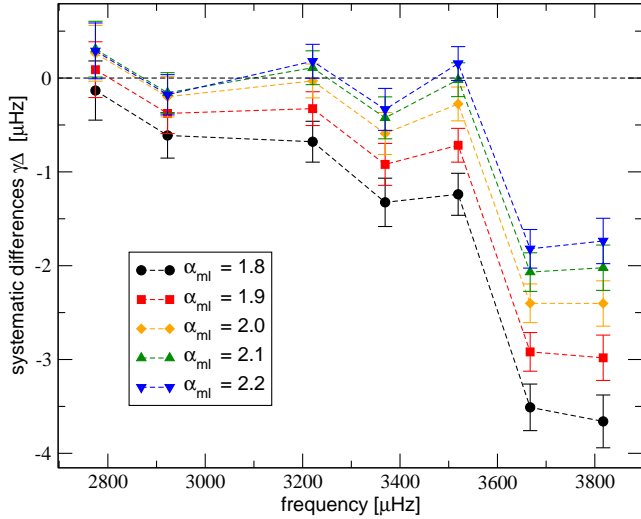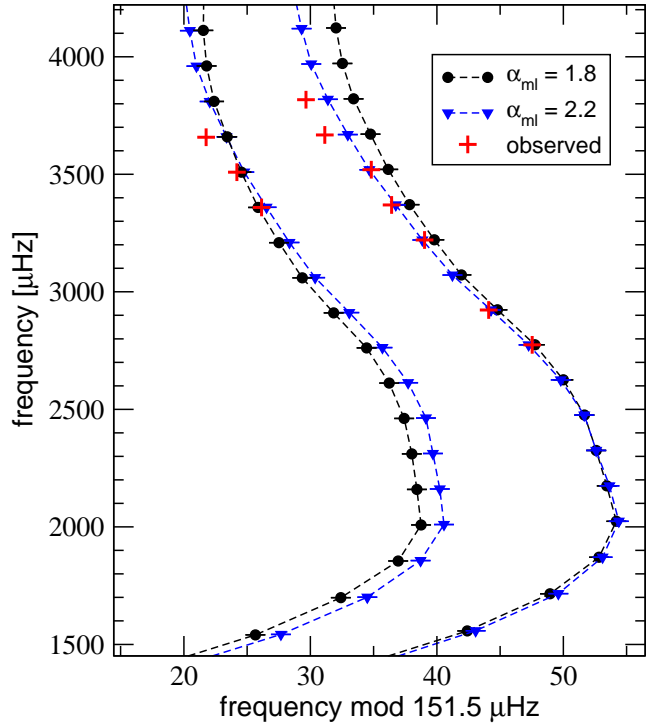
Figure 1. Systematic differences between observed and computed $l = 0$ modes for KIC 8006161 when fitted by models with varying mixing length but otherwise fixed initial parameters.


Figure 2. Echelle diagrammes for the l=0 (right sequence) and 2 (left sequence) modes of KIC 8006161 and two models with different α_{ml}. The uncertainties of the observed frequencies are of the order of the symbol size.

metallicity, T_{eff} and L can be estimated from spectroscopic and photometric observations. Furthermore, equation 1 reveals that ν_{max} provides valuable if approximate constraints for the fundamental parameters, including the stellar mass, in particular when spectroscopic constraints are available.

Two adjustable parameters of the stellar model, the helium abundance and α_{ml}, affect the structure of the surface layers. The mixing length parameter is normally tuned to produce a model of the Sun at the observed composition and (meteoritic) age that matches the limb-darkening-corrected radius of the Sun. The helium abundance is either derived also from a tuned model of the Sun, matching its luminosity, or extrapolated from the observed rate of Galactic nucleosynthesis. Both the helium abundance and the α_{ml} affect the depth of the convection zone (i.e., the fitted adiabat) and the temperature gradient in the superadiabatic layer (SAL)[4] via the mixing length theory. We stress that the mixing length parameter of the MLT is used primarily to control the efficiency of convection and its adjustment is primarily used to fix the radius of the star. As is well known for the case of the Sun the MLT does not correctly predict the temperature gradients in the SAL so even though it may be providing an accurate radius for the star it may, at the same time, be providing a poor model of the SAL (e.g., Robinson et al. 2003). The surface effect is sensitive to α_{ml} since the p-mode frequencies are sensitive to the SAL. But at the same time the large frequency spacings are also sensitive to the α_{ml} via its effect on the star's radius. The interplay of the two effects of the mixing length parameter on the frequencies makes it difficult to isolate the surface effect completely from α_{ml}.

Figure 1 shows the effect of fitting one of the stars in our sample, KIC 8006161, to a specific evolutionary track with $M = 1.11\,M_\odot$, $Y_0 = 0.22$ and $Z_0 = 0.04$, but varying values of α_{ml} (note that these models are not equivalent to our most probable models as determined in the next section). At the highest frequencies, the larger α_{ml} values clearly reduce the measured surface effect by almost 50%, and the effect is even more pronounced at the lower orders.[5] On the other hand, the plot suggests that at the lowest observed radial order, the frequencies for the higher-α_{ml} models are somewhat too low. Figure 2 presents the echelle diagramme for the l=0,2 modes of the $\alpha_{\mathrm{ml}} = 1.8$ and $\alpha_{\mathrm{ml}} = 2.2$ models. We observe that if the set of l=2 modes extended below $\sim 3000\,\mu$Hz, we would be able to clearly distinguish between these two models. At the l=0 orders below $\sim 2000\,\mu$Hz the two models show small but systematic differences as well. With the current set of observed modes, however, we cannot clearly determine whether a lower or higher mixing length parameter value is more probable. Yet, we want to find the model with the smallest surface effects that still fits all other constraints. Therefore, in our example the higher α_{ml} values become more probable automatically. As long as we have limited knowledge on the magnitude of the surface effects across the HR diagram, however, this increase in probability might not be warranted. In the given example, it does seem as if the $\alpha_{\mathrm{ml}} = 2.2$ model is more consistent with the observed small spacing, but we know that the solar-calibrated value is closer to $\alpha_{\mathrm{ml}} \sim 1.8$, so deviations from this value should not be taken lightly[6]. Nonetheless, studying the pos-

---

[4] Below the SAL, the temperature gradient is adiabatic.

[5] It is necessary to point out, however, that for adiabatic frequencies, the relative impact of the mixing length is not as big as for the non-adiabatic frequencies.

[6] Note that such deviations are also a non-negligible problem when applying the standard surface correction since it relies on the solar-calibrated values at the solar mixing length parameter.
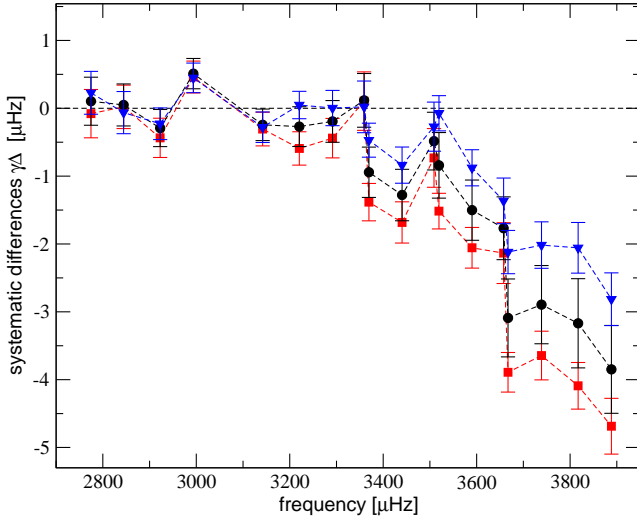
Figure 3. Systematic differences between all observed and computed modes of KIC 8006161 for the whole grid, calculated with (black circles) and without (blue triangles) α_{ml} prior. Results for only the $\alpha_{\mathrm{ml}} = 1.8$ models (red squares) are also shown.

sible variation of the mixing length parameter across the HRD and its interplay with the surface effects is important, so setting a fixed (calibrated) value is also not desirable.

We therefore propose the following solution: we perform our analysis using three different approaches to constraining the mixing length. The first approach is to not use any prior on α_{ml}. The second approach is to employ a Gaussian prior with $\alpha_{\mathrm{ml}} = 1.8 \pm 0.075$, based on the solar calibrated value. The standard deviation of the prior (0.075) is somewhat arbitrary, but we choose it to permit deviations from the calibrated value in the presence of strong evidence. As the maximum value of α_{ml} in our grid is 2.4, such a model would represent an *a priori* 8σ outlier. For such a model to still be more probable, it would require differences in likelihood of about 14 orders of magnitude, and therefore a large amount of evidence from the frequencies and the fit to the other stellar parameters. The prior should therefore only lead to $\alpha_{\mathrm{ml}} > 2.1$ for stars that can be matched very well both in terms of their frequencies and in terms of their fundamental parameters. Lastly, the third approach is to constrain ourselves to $\alpha_{\mathrm{ml}} = 1.8$ in reference to the Sun-calibrated value for Eddington atmospheres. This set of different constraints on α_{ml} will allow us to show its impact on the stellar parameters and the surface effects. By comparing the Bayesian evidence for the result obtained with different priors, we can also quantify the formal preference of one prior over the others.

As an example, we present the results for the surface effect analysis of KIC 8006161, based on the complete grid rather than just one evolutionary track, in Figure 3. While for this star the prior does not have a big effect at the lower order modes, we obtain significantly larger surface effects beyond $3300\,\mu$Hz with the α_{ml} priors. Even with the Gaussian α_{ml} prior, as will be shown below, the most probable posterior value for α_{ml} lies above 1.8.
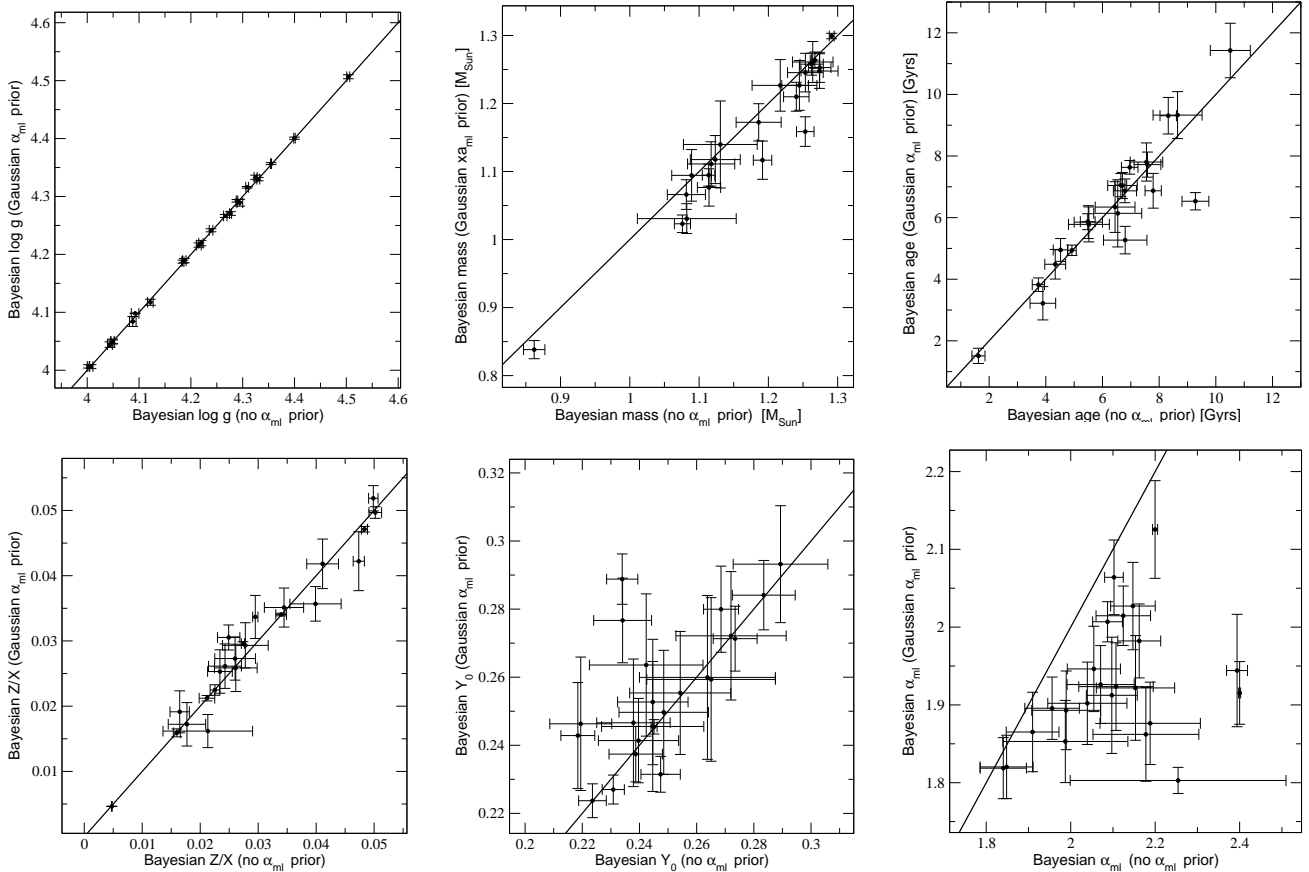
4 RESULTS

As described in the previous sections, we have analysed all 23 stars in our sample with the same grid, using priors on their fundamental parameters if available and three different models relating to the treatment of systematic errors. Moreover, we perform this analysis three times, first setting $\alpha_{\mathrm{ml}} = 1.8$, then with a Gaussian prior, and lastly without a prior on α_{ml}. The results are given in Table 1, Table 1, and Table 1, and the most probable α_{ml} priors and surface effect models are also indicated.

4.1 The influence of the α_{ml} priors

Before we move on to a comparison to the literature, we first study the effect of the α_{ml} priors on our results. Figure 4 shows the posterior mean values and uncertainties of α_{ml}, M, Y_0, $\log g$, Z/X, and age for all stars and compares the results with and without the Gaussian α_{ml} prior. The Gaussian α_{ml} prior leads to slightly lower values of α_{ml} as was expected from the discussion in Section 3. Furthermore, the stellar masses are also slightly lower with an average difference $\langle \Delta M \rangle = -0.021\,\mathrm{M}_\odot$, and, although there is a larger scatter in Y_0, slightly larger values in the initial helium mass fraction are also preferred with an average difference of $\langle \Delta Y_0 \rangle = 0.008$. On the other hand, $\log g$ remains basically unaffected as expected, since the radius of the stars are well constrained by the large spacings (as we will see below, this also extends to a comparison with the other α_{ml} prior and the literature). Z/X and age also do not show strong systematic effects. Nonetheless, the latter does exhibit a strong outlier with 16 Cyg B, for which the age changes from $9.279 \pm 0.473\,\mathrm{Gyrs}$ to $6.532 \pm 0.281\,\mathrm{Gyrs}$. Note that even though the Bayesian evidence is clearly in favour of the older model, the younger value is much more reasonable, given the results from Metcalfe et al. (2012) and also given the value of the age for 16 Cyg A. This is a good test case for the impact of the α_{ml} prior.

A comparison of the results from the Gaussian prior and the fixed $\alpha_{\mathrm{ml}} = 1.8$ prior is presented in Figure 5. In general, the results fall in line with our expectations: the mass is now slightly larger for the Gaussian prior with $\langle \Delta M \rangle = 0.014$, and Y_0 is slightly smaller with $\langle \Delta Y_0 \rangle = -0.005$. Z/X and age values are again quite comparable except for a few outliers. In general the systematic differences between the Gaussian prior and the $\alpha_{\mathrm{ml}} = 1.8$ prior results are smaller than those obtained in a comparison without any priors on α_{ml}. Overall, our comparison reveals that stronger constraints on α_{ml} do not perturb the parameters outside the uncertainties and produce slightly lower stellar masses and higher Y_0.

In terms of the systematic errors, in particular the surface effect, the results also follow our conclusions from the previous section. Figure 6 shows the differences in the systematic errors that arise by using the two α_{ml} priors for every mode of every star in our sample. Using the Gaussian α_{ml} prior leads to an increase in the magnitude of the surface effects (= more negative systematic differences between observed and calculated frequencies) in general. There are only a few stars in the sample for which the effect is very pronounced. It is interesting that for many modes the Gaussian α_{ml} prior does not produce large differences for the surface effects. This is due to the fact that we find a number of stars

Figure 4. The effect of the Gaussian α_{ml} prior on the posterior value of various model parameters. Results are plotted for the most probable systematic error model as given in, e.g., Table 1. The black line indicates a ratio of unity.

for which the surface effects are not significant unless we restrict the analysis to the $\alpha_{ml} = 1.8$ models. Consequently, switching to the $\alpha_{ml} = 1.8$ prior results in even bigger surface effects and to significant surface effects for more stars in the sample. This is also reflected in the strong preference for the SSE model, as shown in the result tables. In both panels there are also a few outliers for which the priors lead to decreased surface effects (= more positive systematic differences between observed and calculated frequencies), but these modes belong to the stars for which the ASE model is either preferred or very similar in probability to the surface effect model.

As indicated in our result tables, using no α_{ml} prior often leads to the highest evidence. Larger evidence values require that the models are formally more consistent with all our available constraints while also minimizing the systematic errors, i.e., the surface effects. Therefore, the analysis which yields the highest evidence and thus the corresponding stellar parameters are usually interpreted as being most appropriate. As explained in Section 3, however, we stress that at this point it is necessary to present the results from all approaches, and not to put too much confidence into the formal preference over to α_{ml} priors. This follows simply because we do not possess enough low-order modes or additional information to anchor the surface effect relation. The only clear exception to this are KIC 8379927 and KIC 10516096, for which we do not detect significant system-

atic errors irrespective of the α_{ml} priors but still find higher α_{ml} to be most probable. Concerning the impact of α_{ml} on the other stellar parameters, however, only the stellar mass and Y_0 seem to be somewhat systematically affected by the choice of priors. Even for those parameters the deviations are usually within the quoted uncertainties. Thus, for our comparison with the values published in the literature, which also allow different values of α_{ml}, we constrain ourselves to the results obtained using the "intermediate approach", the Gaussian α_{ml} prior, and refer to our tabulated results for the differences arising from the different priors.

4.2 Surface effects and other systematic frequency differences

As previously alluded to, Figure 6 suggests that many stars do not show strong evidence for surface effects when our non-adiabatic models are used in tandem with the Gaussian prior. The situation changes, however, when the $\alpha_{ml} = 1.8$ prior is used. This implies that, depending on the prior, the convective contributions to the surface effects are either more or less significant. Since a proper normalization of the surface effect amplitudes is not trivial and the shape of the surface effects can vary from star to star, we instead quantify the significance of the surface effect in terms of probabilities. As discussed in Section 2.3, our calculations consider three different systematic error models: SSE, ASE, and NSE.
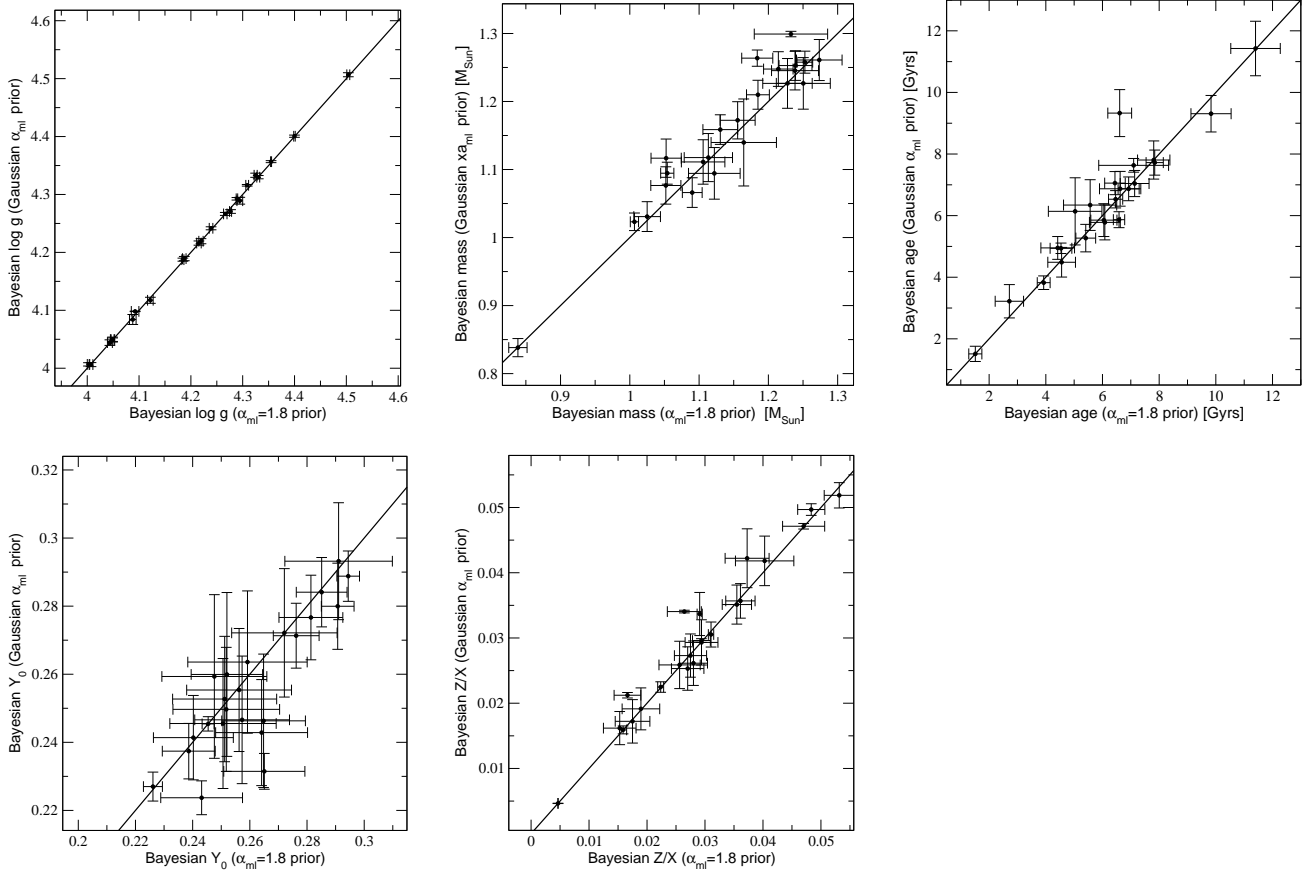
Figure 5. Same as Figure 4 but for the $\alpha_{\mathrm{ml}} = 1.8$ prior and the Gaussian α_{ml} prior. Comparison of α_{ml} is not shown.

Therefore, in order to quantify the surface effect significance for every star, we simply calculate the odds ratio

$$ODDS = \frac{ev(SSE)}{ev(ASE) + ev(NSE)}, \qquad (5)$$

where $ev(SSE)$, $ev(ASE)$, and $ev(NSE)$ are the evidence values obtained for the analysis using each specific systematic error model[7]. This is the probability ratio between the hypotheses "standard surface effect" and "either arbitrary systematic errors or no systematic errors". Therefore, if surface effects are needed to explain the observations, we expect that $ODDS \gg 1$. According to the convention established by Jeffreys (1961), the evidence for or against one of the two hypotheses is considered "substantial" for a factor of 3 to 10, "strong" for a factor of 10 to 30, "very strong" for a factor of 30 to 100, and "decisive" for factors above 100. Hence, when the surface effects become more significant with respect to the other hypotheses, $ODDS$ will increase as well.

Our calculations show that for some stars the significance of the individual systematic error models depend on the specific prior for α_{ml}, in accordance with what was discussed in Section 3. However, there are four stars for which $ODDS < 1$ irrespective of mixing length parameter: KIC 6933899, KIC 8379927, KIC 10516096, and Kepler-36. The

latter three objects do not require any systematic errors at all. Furthermore, for KIC 6106415, KIC 6603624, and KIC 11244118 the surface effect model is only significant for the $\alpha_{\mathrm{ml}} = 1.8$ prior.

Figure 7 shows the actual systematic error measurements obtained when using the Gaussian α_{ml} prior that have been rescaled and plotted as a function of their mean α_{ml}. For many stars the individual deviations do not seem to correspond to the clear power-law behaviour that can be identified for the Sun. Furthermore, there appears to be a very weak dependence on α_{ml}, where higher values are related to smaller normalised surface effects, as expected from the discussion in Section 3. Whether this dependence is physically meaningful depends on whether these stars actually have higher values of α_{ml}, or if it is simply the case that our α_{ml} prior is too weak. In any case, α_{ml} and surface effects are related.

Similar to Mathur et al. (2012), we do not find any simple correlations of the normalised surface effect with any of the other parameters in Table 1 to Table 1. However, studying the *significance* of the surface effect in terms of probabilities reveals some interesting results. Figure 8 shows the logarithm of the odds ratio for all stars in our sample as a function of their position in the HR diagram. The most significant detections appear to be situated at close-to-solar values of T_{eff} and the picture is similar whether the Gaussian α_{ml} prior, the $\alpha_{\mathrm{ml}} = 1.8$ prior, or no α_{ml} prior is used. Furthermore, the coolest star in the sample, KIC 8006161, also dis-

---

[7] This assumes that *a priori* all three surface effect models are equally probable.
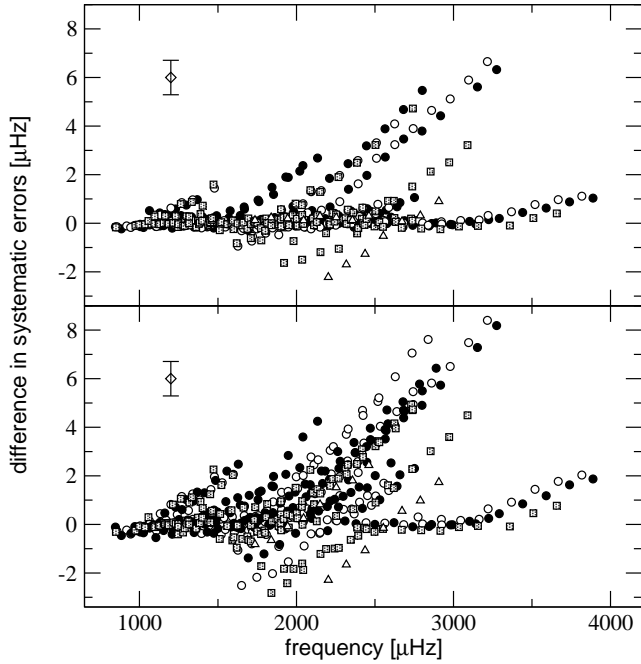
Figure 6. Differences in the measured systematic errors that arise from using the Gaussian α_{ml} prior (top panel) or the $\alpha_{ml} = 1.8$ prior (bottom panel). All modes of all stars are shown: l=0 modes (open circles), l=1 modes (black circles), l=2 modes (shaded squares), and l=3 modes (open triangles). Positive (negative) values denote bigger (smaller) systematic errors in terms of surface effects when the α_{ml} priors are used. The average uncertainty of the differences is indicated by the diamond in the upper left. For each star, the plotted differences were obtained using the most probable systematic difference model for the respective α_{ml} prior.

plays highly significant surface effects but lies far off from the main bulk of the sample. We have also added symbols representing the Sun (Gruberbauer & Guenther 2013), β Hydri (Brandão et al. 2011), and α Cen A& B (Eggenberger et al. 2004), all of which were used by Kjeldsen et al. (2008) to define the surface effect correction. Except for β Hydri[8], the stars fit well into the pattern given by the Kepler stars. 16 Cyg A, 16 Cyg B,α Cen A, and of course the Sun, appear to lie on the "surface effect locus" in the HRD diagram of our sample. α Cen B, on the other hand, is situated very close to KIC 800616.

The stars for which no significant surface effects were detected do mix with stars that show less significant detections, which is why there does not seem to be a strong correlation of the surface effect with any particular parameter. On average, however, lower luminosities and higher effective temperatures correspond to more significant surface effects. Plotting $\log T_{eff}$ against $\log g$ (not shown) necessarily yields a very similar picture which again clusters the most significant detections at the solar values. A correlation of the surface effect amplitude with $\log g$ was already noted by Mathur et al. (2012). Our comparison of the significance of the surface effect would be more in line with their investiga-

---

[8] Note that the surface effects detected in β Hydri have only been measured using adiabatic frequencies which do not contain the correction for radiative gains and losses.
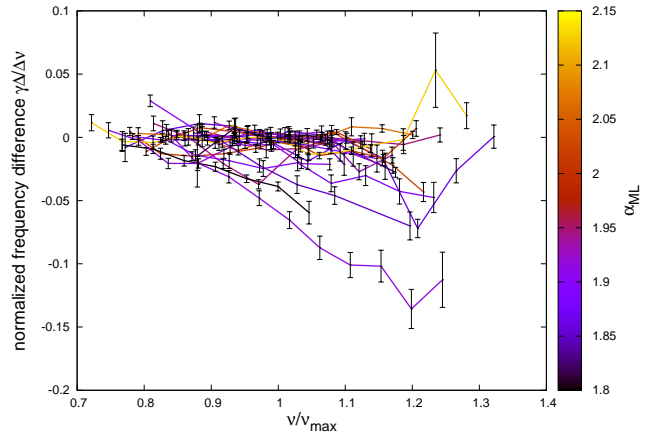
Figure 7. Normalized systematic frequency differences as a function of normalized frequency for $l = 0$ modes for the results obtained with the Gaussian α_{ml} prior. The colour represents the mean posterior α_{ml}. For each star, the plotted differences were obtained using the most probable systematic difference model.
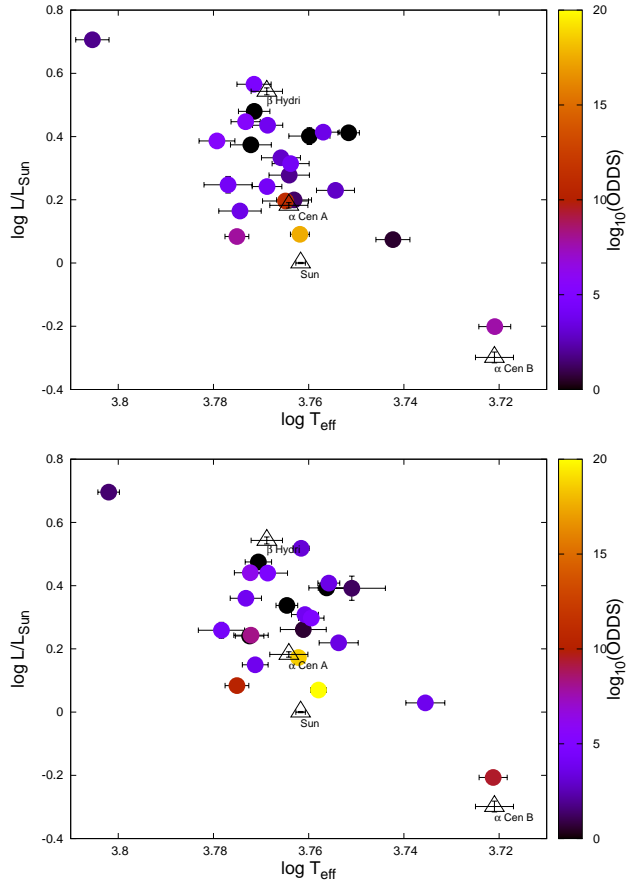
Figure 8. HR diagram of all stars in our sample (filled circles) with parameter taken from Table 1 to Table 1, using the results from the Gaussian (top panel) and $\alpha_{ml} = 1.8$ (bottom panel) prior. The colour indicates the significance of the detected surface effect using $\log_{10}(ODDS)$. Four other well-known stars with surface effects are also shown as triangles. For each star, the plotted parameters were obtained using the most probable systematic difference model for the respective α_{ml} prior.

tion of the normalised surface effect for which they could not find a strong correlation. It will be intriguing to see whether a bigger sample and additional lower order modes could lead to a clearer detection of a "surface effect locus" in the HR diagram.

In any case, the non-detection of surface effects in some stars, as well as the concentration of very significant surface effects for stars with close to solar values should be a warning for unreflected usage of the standard surface correction for all solar-like stars.

4.3   Comparison with non-Bayesian results

4.3.1   Mathur20

In this section we investigate the presence of potential systematic differences between our results and those obtained using the AMP pipeline. Figure 9 shows that there are no strong systematic trends in either of the plotted parameters. As in the comparison between our three different Bayesian analyses (Figure 4, Figure 5), the determined $\log g$ values are very similar, but the Bayesian uncertainties are usually smaller. The results for α_{ml} show large scatter which is mostly compensated by the large uncertainties. It should be noted that our grid only extends from $\alpha_{ml} = 1.8$ to 2.4, and therefore we do not cover the lower values that AMP returns for some of the stars.

The masses that were determined are quite similar for most stars, but the AMP delivers smaller uncertainties on average. For several stars, only the larger uncertainties reported by the Bayesian method can help to reconcile the results. There exists also a clear outlier with KIC 11244118 where the masses differ by about 0.3 $M_\odot$, more than 15 times our statistical uncertainty.[9] The initial helium mass fraction again displays large but seemingly unsystematic scatter, in particular when compared to some of the uncertainties reported by AMP. Many of the stars appear to prefer very low values of Y_0, as was also found to be the case by Mathur et al. (2012). However, for these stars our various approaches (different α_{ml} priors, different systematic error models) can often provide a solution with higher values albeit lower evidence. Also, in many cases the Bayesian uncertainties are usually large enough to reconcile the values with those required from studies of Big Bang nucleosynthesis. The only clear outlier here is KIC 8379927 for which we find quite large disagreements with the AMP results. Contrary to the somewhat larger discrepancies for Y_0, the results for Z/X are more similar, but our values appear to be slightly larger in a systematic way. In general, we have to stress that concerning the chemical composition, our grid is quite coarse compared to the capabilities of AMP's genetic algorithm.

Lastly, significant differences appear in the comparison of the determined ages. Irrespective of potential differences in the definition of zero-age models, the two methods yield different results with significant scatter. Moreover, the Bayesian age uncertainties appear to be bigger on average by a factor of 6, which is substantial, necessary, but insufficient to reconcile the results in many cases.

We re-emphasize that the Bayesian uncertainties are properly propagated through the whole grid and also include the effects of the systematic frequency differences (via marginalisation) and any non-asteroseismic constraints (via the prior probabilities). AMP, on the other hand, can only consider statistical contributions to the uncertainties. While dependent on the particular grid that was analysed, the Bayesian uncertainties are therefore superior from a methodological point of view. This different approach, as well as differences in the stellar models themselves, is sufficient to explain the reported discrepancies.

4.3.2   16 Cyg A & B

The modelling performed by Metcalfe et al. (2012) revealed that 16 Cyg A & B are of slightly different masses but have a similar age, as expected for a binary system. Several different grids and methods were used, including AMP, to arrive at an average ensemble solution. Our results compare favourably with this ensemble average, when it comes to the ages, the masses, Z_0, and α_{ml}. Except for the mass of 16 Cyg B, for which we obtain $1.023 \pm 0.013\, M_\odot$ compared to their result of $1.07 \pm 0.02\, M_\odot$, these parameters overlap within their respective 1σ uncertainties. It should be noted that we obtain a lower mass for 16 Cyg A as well, which might suggest a systematic difference between the methods and models used. As discussed in the previous section, however, we don't find that such a trend is true for our larger sample. The ages are fully consistent with a common origin, even though this constraint was not used in the analysis[10].

We find a slight discrepancy for the initial helium mass fraction. For 16 Cyg A we obtain $Y_0 = 0.282 \pm 0.01$ and for 16 Cyg B we find $Y_0 = 0.285 \pm 0.01$, while Metcalfe et al. report 0.25 ± 0.01. Overall, we observe that the differences between our results and the ensemble average in the literature are minor.

Comparing our results exclusively to the AMP values, we see a significant difference in the age and the value of α_{ml} for 16 Cyg B. It is interesting that this star is among the set of the most significant surface-effect detections in our sample. As the AMP results in a value of $\alpha_{ml} = 2.05 \pm 0.03$, which is bigger than the ensemble average, it is perhaps the combination of the solar-calibrated surface effect correction and the use of a higher-than-solar α_{ml} which results in the discrepancy. For the age, we obtained 6.532 ± 0.281 Gyr compared to 5.8 ± 0.1. Consistent with our findings in Section 4.3.1, we observe that our age uncertainties are significantly bigger.

In a recent paper, White et al. (2013) have combined interferometric diameters from CHARA observations with Hipparcos parallaxes, spectrophotometric bolometric fluxes, and the asteroseismic large frequency separation, to obtain largely model-independent constraints for 16 Cyg A & B. In comparison to their results, for 16 Cyg A, our $\alpha_{ml} = 1.8$ prior produces a very close match in terms of mass and radius, but the model $T_{\rm eff}$ values are slightly too low and match better for the Gaussian α_{ml} prior. For 16 Cyg B, on

---

[9] This star is also problematic since it fits best to models near the border of our grid both in terms of mass and metallicity.

[10] The equal age is in even better agreement with our results for the $\alpha_{ml} = 1.8$ prior, but for this approach we also obtain substantially smaller masses.
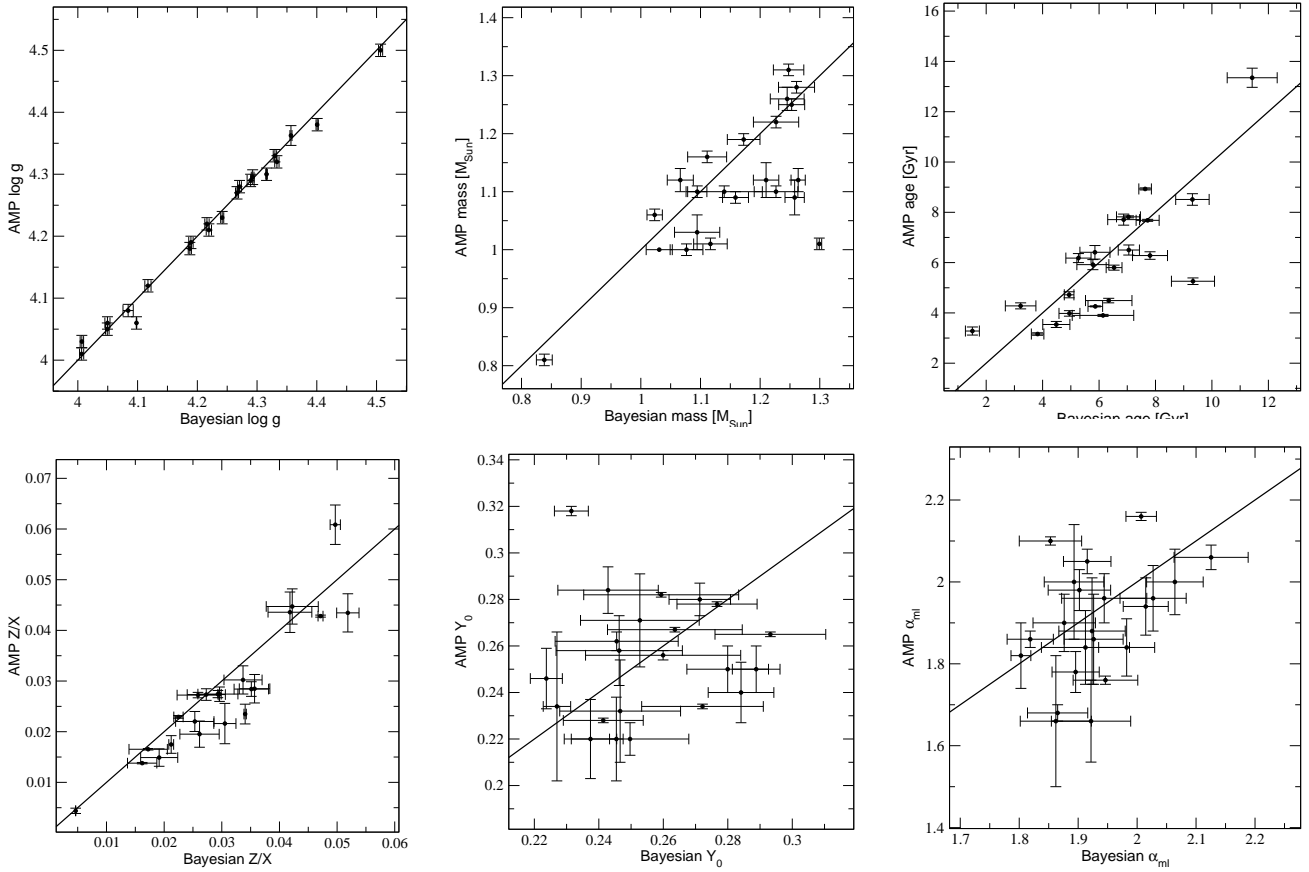
Figure 9. Same as Figure 4 but comparing the results from our Bayesian approach using the α_{ml} prior with the published results obtained via the AMP pipeline (Mathur et al. 2012; Metcalfe et al. 2012). Note that Kepler-36 is not included in these plots.

the other hand, the higher α_{ml} values are more consistent with their results, predicting higher masses and larger radii but again T_{eff} values that are not quite high enough to match the mean observed values. These slight differences however are insignificant and, irrespective of the particular priors used, we find that our results match the masses, temperatures, and radii from White et al. (2013) reasonably well and in all cases to within the combined 1.5σ uncertainties. Therefore, the interferometric uncertainties are too large to give strong evidence for or against our particular solutions (i.e., in particular the different α_{ml} values). This can also be interpreted as additional justification for the various α_{ml} priors, since the range of results allows us to define a parameter space that is more in line with model-independent observations.

4.3.3 Kepler-36

With respect to Kepler-36, we find that we can match all parameters published in Carter et al. (2012) within the uncertainties. It is interesting, however, that we do not detect any surface effects for this star. Carter et al. report that the surface-effect correction was applied to the frequencies. Judging from our results, any surface effects necessary to be corrected for this star would have to originate from the radiative losses that are already taken into account in our non-adiabatic models.

5   CONCLUSIONS

In this paper we have reported on our asteroseismic analysis of 23 previously published stars that were observed with the Kepler satellite. We compared the results obtained with our Bayesian grid-based method to the results from the literature, most importantly those obtained with the AMP. Except for a weak trend towards larger values of Z/X with our method, no obvious systematic differences in the basic stellar parameters can be found. In part, this is certainly due to spectroscopic constraints (T_{eff}, $\log g$, $[Fe/H]$, $L/L_{\odot}$) that were used by all authors.

However, we observe that the uncertainties derived from the two methods differ substantially for some stellar parameters. Uncertainties in the stellar ages in particular are either significantly underestimated by AMP or significantly overestimated by the Bayesian method. We conclude that the flexible treatment of the surface effects in the Bayesian approach is probably responsible for this discrepancy. Different values of α_{ml} and the usage of non-adiabatic models require a more flexible treatment of the surface effect. Therefore, in our view the uncertainties derived with our method more adequately represent our actual state of knowledge about the surface effects and are therefore more realistic. On the other hand, the interplay between the surface effect and α_{ml} introduces another layer of complexity in the analysis which has to be taken into account in the determination of the stellar

parameters. We propose that future studies with more stars should aim to reexamine this interdependence, especially as long as non-seismic constraints on α_{ml} are not available.

Concerning the surface effects themselves, we find that with a Gaussian prior on α_{ml}, only a few stars in our sample actually require larger corrections. 6 stars in our sample do not show strong evidence for any surface effect at all. Compared to the results in Mathur et al. (2012), this suggests that for many stars taking into account the radiative losses is already good enough. On the other hand, using only models with $\alpha_{ml} = 1.8$ leads to more significant detections. Irrespective of the prior on α_{ml}, we also discovered that the stars for which we do find a highly significant surface effect appear to be located very close to the Sun in the HR diagram (see Figure 8). A comparison with the stars that were used to derive the traditional surface-effect correction (Kjeldsen et al. 2008) shows that most of these calibrators - including the Sun - also fit the picture. As radiative losses are already taken into account in our models, the modelling of convection and its dependencies on element abundances, opacities, and the equation of state remains a leading candidate to explain the cause of the surface effects.

To conclude, although systematic differences between stellar evolutionary codes are still affecting the individual stellar parameters, the systematic analysis of surface effects can already be pursued using more advanced methods than the standard surface correction, such as our Bayesian approach. No matter which surface correction is used, however, the constraints on α_{ml} will potentially affect the results in the absence of lower-order modes. The data sets on which this analysis is based have since been superseded by many more quarters of Kepler data. Also, many more stars have been observed, for which public frequencies are also available (Appourchaux et al. 2012). Strong spectroscopic constraints and access to lower-order modes will be necessary to improve our analysis, and to see whether the "surface effect locus" can be reproduced with a larger sample of stars and better data. Given the large number of subgiants and red giants observed with *Kepler* and CoRoT, a similar study for non-main sequence stars could be very illuminating as well.

REFERENCES

Alexander D. R., Ferguson J. W., 1994, ApJ, 437, 879
Appourchaux T. et al., 2012, A&A, 543, A54
Bahcall J. N., Pinsonneault M. H., Basu S., 2001, ApJ, 555, 990
Bahcall J. N., Pinsonneault M. H., Wasserburg G. J., 1995, Reviews of Modern Physics, 67, 781

Bahcall J. N., Ulrich R. K., 1988, Reviews of Modern Physics, 60, 297
Böhm-Vitense E., 1958, ZAp, 46, 108
Borucki W. J. et al., 2010, Science, 327, 977
Brandão I. M. et al., 2011, A&A, 527, A37+
Carter J. A. et al., 2012, Science, 337, 556
Chandrasekhar S., 1957, An introduction to the study of stellar structure.. Dover Publications, New York
Chaplin W. J. et al., 2011, Science, 332, 213
Demarque P., Guenther D. B., Li L. H., Mazumdar A., Straka C. W., 2008, Ap&SS, 316, 31
Eggenberger P., Charbonnel C., Talon S., Meynet G., Maeder A., Carrier F., Bourban G., 2004, A&A, 417, 235
Feroz F., Hobson M. P., Bridges M., 2009, MNRAS, 398, 1601
Grigahcène A., Dupret M.-A., Sousa S. G., Monteiro M. J. P. F. G., Garrido R., Scuflaire R., Gabriel M., 2012, MNRAS, 422, L43
Gruberbauer M., Guenther D. B., 2013, MNRAS
Gruberbauer M., Guenther D. B., Kallinger T., 2012, ApJ, 749, 109
Guenther D. B., 1994, ApJ, 422, 400
Guenther D. B., Brown K. I. T., 2004, ApJ, 600, 419
Hayashi C., 1961, PASJ, 13, 450
Huber D. et al., 2011, ApJ, 743, 143
Iglesias C. A., Rogers F. J., 1996, ApJ, 464, 943
Jeffreys H., 1961, Theory of Probability, third edn. Oxford University Press, Oxford, England
Kallinger T. et al., 2010, A&A, 522, A1
Kjeldsen H., Bedding T. R., Christensen-Dalsgaard J., 2008, ApJ, 683, L175
Lane J. H., 1869, Amer. J. Sci., 2nd ser., 50, 57
Mathur S. et al., 2012, ApJ, 749, 152
Metcalfe T. S. et al., 2012, ApJ, 748, L10
Metcalfe T. S., Creevey O. L., Christensen-Dalsgaard J., 2009, ApJ, 699, 373
Metcalfe T. S. et al., 2010, ApJ, 723, 1583
Michel E. et al., 2008, Science, 322, 558
Miglio A. et al., 2013, MNRAS, 429, 423
Palla F., Stahler S. W., 1999, ApJ, 525, 772
Robinson F. J., Demarque P., Li L. H., Sofia S., Kim Y.-C., Chan K. L., Guenther D. B., 2003, MNRAS, 340, 923
Rogers F. J., 1986, ApJ, 310, 723
Rogers F. J., Swenson F. J., Iglesias C. A., 1996, ApJ, 456, 902
White T. R. et al., 2013, MNRAS, in press, arXiv 1305.1934

Table 1. Mean parameters and uncertainties as a function of α_{ml} prior for KIC 3632418 to KIC 6603624. Bold font indicates the prior for which the highest evidence was obtained, as well as other priors for which the evidence was comparable (within a factor of 5). Y_0, Z_0: initial helium and metal mass fractions; Z_s: metal mass fraction in the envelope; R_{BCZ}: fractional radius of the base of the convection zone; α_{ml}: mixing length parameter; sys: the most probable systematic-error model is given (SSE = standard surface effect, ASE = arbitrary systematic errors, NSE = no systematic errors) and asterisks indicate a probability contrast of less than an order of magnitude with respect to any of the other systematic-error models.

Star	α prior	$M/M_\odot$	$\log T_{\mathrm{eff}}$	$\log L/L_\odot$	$\log R/R_\odot$	Age	Y_0	Z_0	Z_s	Z_s/X_s	R_{BCZ}	α_{ml}	sys
3632418	**$\alpha_{\mathrm{ml}} = 1.8$**	1.273	3.802	0.696	0.268	3.926	0.252	0.0134	0.0130	0.0175	0.8397	1.80	SSE
		±0.033	±0.002	±0.007	±0.004	±0.227	±0.012	±0.0024	±0.0022	±0.0030	±0.0069		
	Gaussian	1.261	3.805	0.706	0.266	3.823	0.260	0.0130	0.0126	0.0172	0.8405	1.87	SSE
		±0.030	±0.003	±0.012	±0.004	±0.221	±0.024	±0.0025	±0.0022	±0.0033	±0.0088	±0.05	
	no α_{ml} prior	1.264	3.807	0.713	0.266	3.738	0.264	0.0133	0.0129	0.0177	0.8386	1.91	SSE
		±0.029	±0.003	±0.012	±0.004	±0.217	±0.024	±0.0024	±0.0021	±0.0032	±0.0093	±0.06	
3656476	$\alpha_{\mathrm{ml}} = 1.8$	1.131	3.754	0.219	0.126	6.623	0.281	0.0310	0.0273	0.0373	0.6874	1.80	SSE
		±0.025	±0.004	±0.017	±0.003	±0.729	±0.011	±0.0028	±0.0026	±0.0038	±0.0090		
	Gaussian	1.159	3.754	0.230	0.130	6.871	0.276	0.0347	0.0308	0.0422	0.6732	1.94	SSE
		±0.022	±0.004	±0.017	±0.003	±0.564	±0.012	±0.0034	±0.0031	±0.0045	±0.0089	±0.07	
	no α_{ml} prior	1.253	3.766	0.301	0.143	7.789	0.234	0.0400	0.0359	0.0473	0.6591	2.39	NSE*
		±0.013	±0.002	±0.007	±0.002	±0.287	±0.010	±0.0005	±0.0005	±0.0010	±0.0015	±0.02	
4914923	$\alpha_{\mathrm{ml}} = 1.8$	1.228	3.759	0.297	0.154	5.409	0.259	0.0306	0.0271	0.0361	0.7097	1.80	SSE
		±0.036	±0.003	±0.013	±0.004	±0.349	±0.021	±0.0017	±0.0016	±0.0025	±0.0078		
	Gaussian	1.227	3.764	0.314	0.153	5.269	0.263	0.0299	0.0266	0.0357	0.7075	1.88	SSE
		±0.037	±0.004	±0.018	±0.004	±0.446	±0.021	±0.0018	±0.0017	±0.0026	±0.0092	±0.05	
	no α_{ml} prior	1.245	3.769	0.343	0.157	6.802	0.242	0.0337	0.0302	0.0399	0.6812	2.19	SSE
		±0.025	±0.005	±0.021	±0.003	±0.766	±0.020	±0.0035	±0.0032	±0.0044	±0.0102	±0.12	
5184732	$\alpha_{\mathrm{ml}} = 1.8$	1.239	3.761	0.261	0.132	4.421	0.277	0.0394	0.0350	0.0483	0.7258	1.80	SSE*
		±0.024	±0.005	±0.023	±0.003	±0.594	±0.008	±0.0016	±0.0015	±0.0023	±0.0143		
	Gaussian	1.253	3.764	0.278	0.135	4.951	0.271	0.0400	0.0360	0.0497	0.6995	2.03	SSE
		±0.022	±0.004	±0.020	±0.003	±0.370	±0.010	±0.0004	±0.0004	±0.0009	±0.0070	±0.06	
	no α_{ml} prior	1.274	3.771	0.312	0.137	4.521	0.273	0.0399	0.0362	0.0502	0.7022	2.15	SSE
		±0.016	±0.003	±0.016	±0.002	±0.257	±0.008	±0.0007	±0.0006	±0.0011	±0.0049	±0.05	
5512589	**$\alpha_{\mathrm{ml}} = 1.8$**	1.106	3.756	0.408	0.216	7.843	0.272	0.0222	0.0192	0.0256	0.6620	1.80	SSE
		±0.031	±0.002	±0.008	±0.004	±0.303	±0.018	±0.0026	±0.0024	±0.0036	±0.0051		
	Gaussian	1.111	3.757	0.414	0.217	7.722	0.272	0.0223	0.0194	0.0259	0.6629	1.82	SSE
		±0.033	±0.003	±0.015	±0.004	±0.408	±0.019	±0.0026	±0.0024	±0.0036	±0.0054	±0.04	
	no α_{ml} prior	1.117	3.758	0.421	0.218	7.588	0.272	0.0225	0.0196	0.0261	0.6640	1.84	SSE
		±0.034	±0.004	±0.019	±0.004	±0.472	±0.019	±0.0026	±0.0025	±0.0037	±0.0057	±0.05	
6106415	$\alpha_{\mathrm{ml}} = 1.8$	1.184	3.772	0.243	0.101	4.536	0.243	0.0236	0.0204	0.0264	0.7446	1.80	SSE
		±0.022	±0.004	±0.014	±0.003	±0.383	±0.014	±0.0023	±0.0021	±0.0029	±0.0088		
	Gaussian	1.264	3.772	0.264	0.112	4.939	0.224	0.0300	0.0265	0.0341	0.7174	2.06	NSE
		±0.012	±0.002	±0.010	±0.001	±0.170	±0.005	± < 0.0001	±0.0001	±0.0002	±0.0038	±0.05	
	no α_{ml} prior	1.267	3.774	0.271	0.112	4.922	0.223	0.0299	0.0265	0.0340	0.7163	2.10	NSE*
		±0.007	±0.002	±0.008	±0.001	±0.150	±0.005	±0.0008	±0.0007	±0.0009	±0.0029	±0.02	
6116048	$\alpha_{\mathrm{ml}} = 1.8$	1.090	3.772	0.241	0.099	6.608	0.239	0.0159	0.0132	0.0166	0.7290	1.80	ASE
		±0.014	±0.003	±0.011	±0.002	±0.420	±0.009	±0.0019	±0.0017	±0.0023	±0.0073		
	Gaussian	1.066	3.763	0.200	0.097	9.328	0.237	0.0200	0.0167	0.0212	0.6747	2.01	SSE
		±0.022	±0.004	±0.019	±0.003	±0.763	±0.008	±0.0003	±0.0003	±0.0004	±0.0082	±0.04	
	no α_{ml} prior	1.082	3.770	0.230	0.099	8.650	0.238	0.0197	0.0166	0.0212	0.6789	2.12	SSE
		±0.027	±0.005	±0.024	±0.004	±0.865	±0.009	±0.0012	±0.0010	±0.0013	±0.0100	±0.06	
6603624	$\alpha_{\mathrm{ml}} = 1.8$	1.052	3.735	0.029	0.067	9.830	0.264	0.0356	0.0301	0.0403	0.6625	1.80	SSE
		±0.022	±0.004	±0.015	±0.003	±0.708	±0.016	±0.0040	±0.0034	±0.0050	±0.0057		
	Gaussian	1.117	3.742	0.074	0.076	9.309	0.243	0.0373	0.0319	0.0418	0.6627	1.98	SSE*
		±0.028	±0.004	±0.017	±0.004	±0.593	±0.015	±0.0029	±0.0026	±0.0038	±0.0043	±0.05	
	no α_{ml} prior	1.192	3.751	0.129	0.086	8.321	0.219	0.0371	0.0321	0.0411	0.6687	2.16	NSE*
		±0.013	±0.005	±0.018	±0.002	±0.290	±0.005	±0.0025	±0.0021	±0.0027	±0.0016	±0.05	

Table 1. ... continued.

Star	α prior	$M/M_\odot$	$\log T_{\mathrm{eff}}$	$\log L/L_\odot$	$\log R/R_\odot$	Age	Y_0	Z_0	Z_s	Z_s/X_s	R_{BCZ}	α_{ml}	sys
6933899	$\alpha_{\mathrm{ml}} = 1.8$	1.164 ±0.047	3.756 ±0.004	0.393 ±0.022	0.208 ±0.006	7.808 ±0.571	0.248 ±0.018	0.0245 ±0.0021	0.0212 ±0.0020	0.0275 ±0.0028	0.6779 ±0.0154	1.80	ASE
	Gaussian	1.140 ±0.064	3.760 ±0.004	0.401 ±0.027	0.205 ±0.008	7.806 ±0.620	0.259 ±0.024	0.0237 ±0.0026	0.0207 ±0.0024	0.0273 ±0.0033	0.6650 ±0.0189	1.90 ±0.05	ASE
	no α_{ml} prior	1.131 ±0.053	3.766 ±0.005	0.426 ±0.028	0.204 ±0.007	7.553 ±0.574	0.265 ±0.022	0.0223 ±0.0027	0.0196 ±0.0025	0.0260 ±0.0035	0.6589 ±0.0146	2.04 ±0.09	ASE*
7680114	$\alpha_{\mathrm{ml}} = 1.8$	1.156 ±0.025	3.761 ±0.003	0.309 ±0.010	0.157 ±0.003	6.084 ±0.544	0.286 ±0.009	0.0294 ±0.0018	0.0259 ±0.0017	0.0355 ±0.0025	0.7012 ±0.0068	1.80	SSE
	Gaussian	1.172 ±0.027	3.766 ±0.004	0.333 ±0.017	0.159 ±0.003	5.780 ±0.567	0.284 ±0.010	0.0289 ±0.0022	0.0256 ±0.0020	0.0351 ±0.0030	0.7004 ±0.0076	1.89 ±0.05	SSE
	no α_{ml} prior	1.186 ±0.033	3.771 ±0.005	0.356 ±0.024	0.160 ±0.004	5.521 ±0.721	0.284 ±0.011	0.0281 ±0.0025	0.0251 ±0.0023	0.0345 ±0.0034	0.6997 ±0.0101	1.99 ±0.08	SSE
8006161	$\alpha_{\mathrm{ml}} = 1.8$	1.052 ±0.022	3.721 ±0.003	−0.207 ±0.010	−0.022 ±0.003	2.714 ±0.500	0.265 ±0.015	0.0395 ±0.0015	0.0377 ±0.0015	0.0532 ±0.0026	0.6891 ±0.0026	1.80	SSE
	Gaussian	1.077 ±0.027	3.721 ±0.003	−0.201 ±0.011	−0.019 ±0.004	3.220 ±0.541	0.246 ±0.020	0.0398 ±0.0010	0.0378 ±0.0009	0.0519 ±0.0019	0.6847 ±0.0037	1.91 ±0.07	SSE
	no α_{ml} prior	1.114 ±0.017	3.721 ±0.003	−0.188 ±0.011	−0.013 ±0.002	3.896 ±0.453	0.219 ±0.011	0.0400 ±0.0003	0.0377 ±0.0003	0.0499 ±0.0008	0.6791 ±0.0024	2.10 ±0.06	SSE
8228742	$\alpha_{\mathrm{ml}} = 1.8$	1.214 ±0.021	3.762 ±0.002	0.518 ±0.002	0.260 ±0.003	6.584 ±0.200	0.240 ±0.014	0.0200 ±0.0003	0.0174 ±0.0003	0.0224 ±0.0005	0.6906 ±0.0025	1.80	SSE
	Gaussian	1.248 ±0.025	3.771 ±0.004	0.565 ±0.017	0.264 ±0.003	5.868 ±0.259	0.241 ±0.012	0.0199 ±0.0006	0.0175 ±0.0006	0.0225 ±0.0008	0.6996 ±0.0038	1.95 ±0.05	SSE
	no α_{ml} prior	1.274 ±0.027	3.778 ±0.004	0.596 ±0.017	0.266 ±0.003	5.479 ±0.261	0.240 ±0.014	0.0199 ±0.0006	0.0175 ±0.0006	0.0225 ±0.0008	0.7047 ±0.0039	2.05 ±0.06	SSE
8379927	$\alpha_{\mathrm{ml}} = 1.8$	1.253 ±0.011	3.774 ±0.001	0.184 ±0.007	0.068 ±0.001	1.513 ±0.231	0.226 ±0.003	0.0250 ±0.0003	0.0237 ±0.0003	0.0310 ±0.0005	0.7638 ±0.0039	1.80	NSE*
	Gaussian	1.258 ±0.016	3.778 ±0.004	0.201 ±0.018	0.068 ±0.002	1.511 ±0.248	0.227 ±0.004	0.0246 ±0.0014	0.0233 ±0.0014	0.0305 ±0.0019	0.7651 ±0.0044	1.86 ±0.06	NSE*
	no α_{ml} prior	1.262 ±0.017	3.797 ±0.007	0.279 ±0.029	0.069 ±0.002	1.624 ±0.231	0.231 ±0.004	0.0204 ±0.0014	0.0191 ±0.0014	0.0249 ±0.0019	0.7750 ±0.0060	2.18 ±0.13	NSE*
8760414	**$\alpha_{\mathrm{ml}} = 1.8$**	0.839 ±0.013	3.775 ±0.002	0.084 ±0.014	0.016 ±0.002	11.400 ±0.873	0.245 ±0.002	0.0050 ± < 0.0001	0.0038 ± < 0.0001	0.0046 ± < 0.0001	0.7212 ±0.0090	1.80	SSE
	Gaussian	0.838 ±0.013	3.775 ±0.002	0.084 ±0.014	0.016 ±0.002	11.426 ±0.886	0.245 ±0.002	0.0050 ± < 0.0001	0.0038 ± < 0.0001	0.0046 ± < 0.0001	0.7209 ±0.0092	1.80 ±0.02	SSE
	no α_{ml} prior	0.862 ±0.015	3.789 ±0.008	0.147 ±0.037	0.020 ±0.003	10.511 ±0.706	0.245 ±0.001	0.0050 ± < 0.0001	0.0039 ± < 0.0001	0.0048 ±0.0001	0.7181 ±0.0049	2.25 ±0.26	SSE
10516096	$\alpha_{\mathrm{ml}} = 1.8$	1.185 ±0.017	3.765 ±0.002	0.338 ±0.009	0.163 ±0.002	6.049 ±0.461	0.258 ±0.016	0.0244 ±0.0016	0.0213 ±0.0016	0.0280 ±0.0024	0.7128 ±0.0060	1.80	NSE
	Gaussian	1.210 ±0.021	3.772 ±0.004	0.374 ±0.020	0.166 ±0.003	5.854 ±0.533	0.247 ±0.019	0.0229 ±0.0025	0.0201 ±0.0023	0.0261 ±0.0034	0.7160 ±0.0079	1.92 ±0.06	NSE
	no α_{ml} prior	1.240 ±0.018	3.781 ±0.005	0.419 ±0.022	0.170 ±0.002	5.500 ±0.500	0.238 ±0.013	0.0213 ±0.0022	0.0189 ±0.0020	0.0243 ±0.0028	0.7188 ±0.0072	2.11 ±0.09	NSE
10963065	$\alpha_{\mathrm{ml}} = 1.8$	1.122 ±0.037	3.778 ±0.005	0.259 ±0.025	0.097 ±0.005	5.035 ±0.945	0.252 ±0.018	0.0174 ±0.0025	0.0147 ±0.0023	0.0189 ±0.0032	0.7511 ±0.0167	1.80	SSE
	Gaussian	1.094 ±0.038	3.777 ±0.005	0.248 ±0.026	0.094 ±0.005	6.139 ±1.090	0.252 ±0.18	0.0176 ±0.0025	0.0148 ±0.0022	0.0191 ±0.0032	0.7254 ±0.0198	1.92 ±0.07	SSE
	no α_{ml} prior	1.089 ±0.029	3.785 ±0.005	0.278 ±0.026	0.093 ±0.004	6.538 ±0.846	0.245 ±0.012	0.0154 ±0.0013	0.0129 ±0.0012	0.0165 ±0.0017	0.7162 ±0.0135	2.15 ±0.09	SSE
11244118	$\alpha_{\mathrm{ml}} = 1.8$	1.233 ±0.053	3.751 ±0.007	0.392 ±0.038	0.218 ±0.006	7.100 ±1.232	0.265 ±0.014	0.0388 ±0.0026	0.0345 ±0.0025	0.0470 ±0.0036	0.6830 ±0.0267	1.80	SSE
	Gaussian	1.299 ±0.004	3.752 ±0.002	0.412 ±0.008	0.227 ±0.000	7.633 ±0.222	0.231 ±0.005	0.0400 ±0.0001	0.0359 ±0.0001	0.0471 ±0.0004	0.6557 ±0.0017	2.01 ±0.03	NSE*
	no α_{ml} prior	1.291 ±0.004	3.759 ±0.003	0.438 ±0.011	0.226 ±0.000	6.962 ±0.292	0.247 ±0.007	0.0400 ± < 0.0001	0.0360 ±0.0001	0.0483 ±0.0005	0.6603 ±0.0021	2.09 ±0.04	NSE*
11713510	**$\alpha_{\mathrm{ml}} = 1.8$**	1.025 ±0.019	3.772 ±0.003	0.441 ±0.013	0.200 ±0.003	7.135 ±0.508	0.291 ±0.019	0.0139 ±0.0022	0.0115 ±0.0019	0.0153 ±0.0028	0.6992 ±0.0121	1.80	SSE
	Gaussian	1.031 ±0.022	3.773 ±0.003	0.447 ±0.013	0.201 ±0.003	7.042 ±0.424	0.294 ±0.017	0.0145 ±0.0019	0.0121 ±0.0017	0.0162 ±0.0025	0.6930 ±0.0121	1.85 ±0.05	SSE
	no α_{ml} prior	1.082 ±0.071	3.775 ±0.003	0.467 ±0.025	0.208 ±0.010	6.705 ±0.522	0.290 ±0.016	0.0182 ±0.0057	0.0157 ±0.0055	0.0213 ±0.0077	0.6829 ±0.0138	1.99 ±0.15	SSE*
12009504	$\alpha_{\mathrm{ml}} = 1.8$	1.238 ±0.034	3.773 ±0.003	0.360 ±0.017	0.157 ±0.004	4.558 ±0.488	0.252 ±0.019	0.0239 ±0.0021	0.0207 ±0.0019	0.0270 ±0.0028	0.7451 ±0.0122	1.80	SSE
	Gaussian	1.245 ±0.028	3.779 ±0.004	0.386 ±0.018	0.158 ±0.003	4.487 ±0.480	0.250 ±0.018	0.0223 ±0.0025	0.0195 ±0.0022	0.0253 ±0.0033	0.7419 ±0.0112	1.93 ±0.05	SSE
	no α_{ml} prior	1.253 ±0.026	3.786 ±0.005	0.416 ±0.021	0.159 ±0.003	4.332 ±0.367	0.249 ±0.018	0.0205 ±0.0016	0.0180 ±0.0014	0.0234 ±0.0021	0.7410 ±0.0103	2.07 ±0.08	SSE
12258514	$\alpha_{\mathrm{ml}} = 1.8$	1.250 ±0.039	3.769 ±0.004	0.440 ±0.020	0.206 ±0.004	5.564 ±0.939	0.250 ±0.018	0.0256 ±0.0021	0.0224 ±0.0019	0.0294 ±0.0028	0.7291 ±0.0137	1.80	SSE
	Gaussian	1.227 ±0.038	3.769 ±0.003	0.436 ±0.017	0.204 ±0.004	6.342 ±0.823	0.246 ±0.019	0.0255 ±0.0024	0.0225 ±0.0023	0.0293 ±0.0035	0.7086 ±0.0138	1.90 ±0.04	SSE
	no α_{ml} prior	1.217 ±0.041	3.771 ±0.004	0.445 ±0.020	0.203 ±0.005	6.445 ±0.701	0.245 ±0.018	0.0242 ±0.0029	0.0213 ±0.0027	0.0278 ±0.0039	0.7046 ±0.0134	1.96 ±0.06	SSE

Table 1. ... continued.

Star	α prior	$M/M_\odot$	$\log T_{\mathrm{eff}}$	$\log L/L_\odot$	$\log R/R_\odot$	Age	Y_0	Z_0	Z_{s}	Z_s/X_s	R_{BCZ}	α_{ml}	sys
16CygA	$\alpha_{\mathrm{ml}}=1.8$	1.054	3.762	0.173	0.086	6.441	0.291	0.0250	0.0214	0.0291	0.7027	1.80	SSE
		±0.010	±0.001	±0.006	±0.001	±0.363	±0.006	± < 0.0001	±0.0002	±0.0004	±0.0036		
	Gaussian	1.095	3.765	0.196	0.092	7.055	0.280	0.0281	0.0247	0.0337	0.6730	2.13	SSE
		±0.016	±0.005	±0.023	±0.002	±0.375	±0.012	±0.0024	±0.0021	±0.0033	±0.0056	±0.06	
	no α_{ml} prior	1.114	3.771	0.225	0.095	6.647	0.269	0.0250	0.0220	0.0295	0.6795	2.20	SSE
		±0.009	±0.001	±0.004	±0.001	±0.206	±0.006	±0.0003	±0.0002	±0.0005	±0.0015	±0.01	
16CygB	$\alpha_{\mathrm{ml}}=1.8$	1.007	3.758	0.070	0.043	6.464	0.294	0.0247	0.0214	0.0294	0.6986	1.80	SSE
		±0.006	±0.002	±0.007	±0.001	±0.250	±0.004	±0.0012	±0.0010	±0.0015	±0.0035		
	Gaussian	1.023	3.762	0.091	0.045	6.532	0.289	0.0250	0.0217	0.0296	0.6942	1.92	SSE
		±0.013	±0.002	±0.010	±0.002	±0.281	±0.007	±0.0001	±0.0001	±0.0003	±0.0034	±0.04	
	no α_{ml} prior	1.076	3.764	0.116	0.054	9.279	0.234	0.0250	0.0214	0.0274	0.6621	2.40	SSE
		±0.012	±0.002	±0.009	±0.002	±0.473	±0.005	±0.0001	±0.0001	±0.0003	±0.0035	±0.00	
Kepler36	**$\alpha_{\mathrm{ml}}=1.8$**	1.113	3.771	0.475	0.220	6.923	0.256	0.0150	0.0124	0.0159	0.7059	1.80	NSE
		±0.035	±0.003	±0.015	±0.005	±0.372	±0.018	±0.0004	±0.0004	±0.0006	±0.0121		
	Gaussian	1.118	3.771	0.480	0.221	6.870	0.255	0.0150	0.0125	0.0159	0.7058	1.82	NSE
		±0.035	±0.003	±0.017	±0.005	±0.386	±0.018	±0.0004	±0.0004	±0.0006	±0.0122	±0.04	
	no α_{ml} prior	1.123	3.773	0.486	0.222	6.792	0.254	0.0150	0.0125	0.0160	0.7058	1.85	NSE
		±0.036	±0.004	±0.021	±0.005	±0.409	±0.018	±0.0004	±0.0004	±0.0006	±0.0122	±0.06	